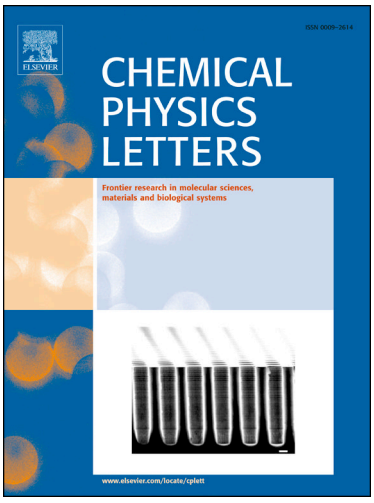

Research paper

Consequences of Theory Level Choice Evaluated with New Tools from QTAIM and the Stress Tensor for a Dipeptide Conformer

Jiahui Li, Tianlv Xu, Yang Ping, Tanja van Mourik, Herbert Früchtl, Steven R. Kirk, Samantha Jenkins

PII: S0009-2614(18)30126-X
DOI: https://doi.org/10.1016/j.cplett.2018.02.041
Reference: CPLETT 35453

To appear in: *Chemical Physics Letters*

Received Date: 23 December 2017
Accepted Date: 13 February 2018

Please cite this article as: J. Li, T. Xu, Y. Ping, T. van Mourik, H. Früchtl, S.R. Kirk, S. Jenkins, Consequences of Theory Level Choice Evaluated with New Tools from QTAIM and the Stress Tensor for a Dipeptide Conformer, *Chemical Physics Letters* (2018), doi: https://doi.org/10.1016/j.cplett.2018.02.041

Consequences of Theory Level Choice Evaluated with New Tools from QTAIM and the Stress Tensor for a Dipeptide Conformer

Jiahui Li[1], Tianlv Xu[1], Yang Ping [1], Tanja van Mourik[2], Herbert Früchtl[2], Steven R. Kirk[*1] and Samantha Jenkins[*1]

[1]*Key Laboratory of Chemical Biology and Traditional Chinese Medicine Research and Key Laboratory of Resource Fine-Processing and Advanced Materials of Hunan Province of MOE, College of Chemistry and Chemical*
[2]*Engineering, Hunan Normal University, Changsha, Hunan 410081, China*
[2]*EaStCHEM School of Chemistry, University of St Andrews, North Haugh, St Andrews, Fife KY16 9ST, Scotland, United Kingdom.*

*email: samanthajsuman@gmail.com
*email:steven.kirk@cantab.net

QTAIM and the stress tensor were used to provide a detailed analysis of the topology of the molecular graph, *BCP* and bond-path properties, including the new introduced helicity length H, of a Tyr-Gly dipeptide conformer subjected to a torsion with four levels of theory; MP2, M06-2X, B3LYP-D3 and B3LYP and a modest-sized basis set, 6-31+G(d). Structural effects and bonding properties are quantified and reflect differences in the BSSE and lack of inclusion of dispersion effects in the B3LYP calculations. The helicity length H demonstrated that MP2 produced a unique response to the torsion suggesting future use as a diagnostic tool.

The analysis of even modest-sized peptide conformers is a difficult problem due to their inherent flexibility, yielding huge numbers of different conformers. It is generally not feasible to study all possible geometries at a high level of theory with large basis sets. Not only do high-level methods scale less favorably with increasing system size, but higher levels of theory require large basis sets to obtain reliable results. For instance, MP2 calculations may produce large basis set superposition error (BSSE) when used with small or moderate-sized basis sets. This may produce more folded and compact conformers because BSSE results in artificial attraction between different parts of the molecule[1–3].

A previous study on the Tyr-Gly dipeptide identified the folded "book1" conformer as the most stable one, based on single-point MP2/6-31+G(d) calculations using B3LYP/6-31+G(d) geometries[4]. A subsequent, more recent, study investigated book1 along the ψ_{tyr} Ramachandran torsion angle profile, and identified an additional minimum around 100° with MP2, M06-2X and B3LYP-D3, but not with B3LYP[5]. The BSSE for this minimum was estimated to be 28.63 (MP2), 6.27 (M06-2X) and 4.28 (B3LYP-D3) kJ/mol.

B3LYP has well known issues with the lack of inclusion of the attractive London dispersion forces, which could be the cause of the lack of a minimum in this region of the B3LYP potential energy surface. On the other hand, the minimum predicted by the other methods could potentially be an artifact of BSSE.

In this investigation we analyze this Tyr-Gly dipeptide conformer subjected to the torsion θ, with these four levels of theory, all with the modest-sized 6-31+G(d) basis set. The purpose of this investigation is not attempting to reduce the large BSSE terms, e.g. by using large basis sets, but instead to better understand the effects of BSSE since intramolecular BSSE is inherently difficult to calculate. Though several methods have been proposed to (approximately) correct intramolecular BSSE[6–12] there is no unique way to do this. Currently, the efforts to understand the unwanted effects of large BSSE solely focus on the location of energy minima and crude insights gained about bonding from the atomic geometries. For example the judgement as to which atoms are bonded, outside of QTAIM, is based purely on geometric separation as is the degree of structural 'compactness'. Instead, we will use the rich topological descriptors available from QTAIM[13] and the stress tensor analysis and we will introduce new concepts to better understand the effects that the BSSE causes without using QTAIM to calculate or predict the BSSE.

For instance, we will track the changing numbers of bond critical points (*BCP*s) and cage critical points (*CCP*s) of the Tyr-Gly dipeptide subject to a torsion θ to assess the level of bonding and compactness of the structure. We also assess the bond strength using the total local energy density $H(\mathbf{r_b})$ and *BCP* stability using the stress tensor eigenvalue $\lambda_{3\sigma}$. In addition, we introduce a new measure to track the excess length that the bond, referred to as the bond-path within QTAIM, possesses as a result of the twisting of the torsional bond, referred to as the *helicity length* H of the bond-path, to find characteristic behaviors of the different levels of theory.

We use QTAIM and the stress tensor analysis, which utilizes higher derivatives of $\rho(\mathbf{r_b})$, acting as a 'magnifying lens' on the $\rho(\mathbf{r_b})$ derived properties of the wave-function. QTAIM[13] allows us to identify critical points in the total electronic charge density distribution $\rho(\mathbf{r})$ by analyzing the gradient vector field $\nabla\rho(\mathbf{r})$.

These critical points can further be divided into four types of topologically stable critical points according to the set of ordered eigenvalues $\lambda_1 < \lambda_2 < \lambda_3$, with corresponding eigenvectors $\underline{\mathbf{e}}_1$, $\underline{\mathbf{e}}_2$, $\underline{\mathbf{e}}_3$ of the Hessian matrix. The Hessian of the total electronic charge density $\rho(\mathbf{r})$ is defined as the matrix of partial second derivatives with respect to the spatial coordinates. These critical points are labeled using the notation (R, ω) where R is the rank of the Hessian matrix, i.e. the number of distinct non-zero eigenvalues, and ω is the signature (the algebraic sum of the signs of the eigenvalues): (3, -3) [nuclear critical point (*NCP*), a local maximum generally corresponding to a nuclear location], (3, -1) and (3, 1) [saddle points, called bond critical points (*BCP*) and ring critical points (*RCP*), respectively] and (3, 3) [the cage critical points (*CCP*)]. The presence of *CCP*s is associated with the resistance of a structure to being crushed[14]. In this investigation, we have closed-shell *BCP*s (H--O *BCP*s, H---H *BCP*s) and shared-shell *BCP*s that comprise the peptide backbone, where the Laplacian $\nabla^2\rho(\mathbf{r}) > 0$ for the closed-shell *BCP*s and $\nabla^2\rho(\mathbf{r}) < 0$ for shared-shell *BCP*s. In the limit that the forces on the nuclei become vanishingly small, an atomic interaction line[15] becomes a bond-path, although not necessarily a chemical bond[16]. The complete set of critical points together with the bond-paths of a molecule or cluster is referred to as the molecular graph.

We can represent the QTAIM topologies of sets of isomers corresponding to allowed, forbidden and unstable solutions to the Poincaré-Hopf relation[17–19] using the quantum topology phase diagram (QTPD)[20–22]. For molecules and clusters, the relation is expressed as:

$$n - b + r - c = 1, \qquad (\mathbf{1})$$

where n, b, r, and c are given by the numbers of *NCP*s, *BCP*s, *RCP*s, and *CCP*s, respectively. For a given collection of isomeric molecular graphs the number of *BCP*s and *RCP*s, given by b and r respectively, contained in each molecular graph are usually plotted along the x-axis and y-axis. In this work however, we will instead plot the torsion angle θ on the x-axis and either b or c on the y-axis. For consistency, we use quantum geometry-centered[23] rather than Euclidean geometry-centered intuition to determine whether a molecular graph is 3-D_{QT}, 2-D_{QT} or 1-D_{QT}, where the subscript '$_{QT}$' is used to denote quantum topology. Molecular graphs of molecules or clusters with one or more *CCP*s will be considered to be quantum topologically 3-D_{QT}. The absence of *CCP*s, but presence of *RCP*s and *BCP*s indicates a 2-D_{QT} molecular graph and without either *CCP*s or *RCP*s a molecular graph will be considered to be 1-D_{QT}. The absence of *CCP*s, *RCP*s and *BC*Ps corresponds to a 0-D_{QT} molecular graph which in turn corresponds to isolated nuclei. The ellipticity ε provides the relative accumulation of $\rho(\mathbf{r_b})$ in the two directions perpendicular to the bond-path at a *BCP*, defined as $\varepsilon = |\lambda_1|/|\lambda_2| - 1$ where λ_1 and λ_2 are negative eigenvalues of the corresponding

eigenvectors. The presence of a degree of covalent character is determined from the total local energy density $H(\mathbf{r}_b)$[24,25], which is defined as:

$$H(\mathbf{r}_b) = G(\mathbf{r}_b) + V(\mathbf{r}_b) \quad \textbf{(2)}$$

In equation **(2)**, $G(\mathbf{r}_b)$ and $V(\mathbf{r}_b)$ are the local kinetic and potential energy densities at a *BCP*, respectively. A value of $H(\mathbf{r}_b) < 0$ for the closed-shell interaction, $\nabla^2\rho(\mathbf{r}_b) > 0$, indicates a *BCP* with a degree of covalent character and conversely $H(\mathbf{r}_b) > 0$ reveals a lack of covalent character for the closed-shell *BCP*.

The quantum stress tensor, $\sigma(\mathbf{r})$, is directly related to the Ehrenfest force by the virial theorem and so provides a physical explanation of the low-frequency normal modes that accompany structural rearrangements[26–28]. There are several versions of the stress tensor in use, but in this investigation we will use Bader's definition[29,30]. A diagonalization of the stress tensor, $\sigma(\mathbf{r})$, returns the principal electronic stresses. The stress tensor eigenvalue associated with the bond-path; $\lambda_{3\sigma}$, has been associated with transition-type behavior in molecular motors[31].

The bond-path length (BPL) is defined as the length of the path of the $\underline{\mathbf{e}}_3$ eigenvector associated with the λ_3 eigenvalue, defined at the *BCP*, of the Hessian of the total charge density $\rho(\mathbf{r})$ that follows the maximum in $\rho(\mathbf{r})$. The bond-path curvature separating two bonded nuclei is defined as the dimensionless ratio:

$$\text{(BPL - GBL)/GBL} \quad \textbf{(3)}$$

where the geometric bond length (GBL) corresponds to the inter-nuclear separation. The BPL often exceeds the GBL particularly for weak or strained bonds and unusual bonding environments[32]. Earlier one of the current authors hypothesized that a bond-path may possess 1-D, 2-D or 3-D topology[33]. Bond-paths possessing zero and non-zero values of the bond-path curvature defined by equation **(3)** can be considered to possess 1-D and 2-D topologies respectively. For some systems subject to an applied torsion θ however, the torsional *BCP* may display negligible variation in the bond-path curvature defined by equation **(3)**. Therefore, a new measure that is more appropriate for bonds with negligible values of the curvature is required. We choose this quantity to be the length traced out in 3-D by the path swept by, for instance, the tips of the scaled $\underline{\mathbf{e}}_2$ eigenvectors of the λ_1 eigenvalue; the scaling factor could be the ellipticity ε. From this we can define a helicity length H, see **Scheme 1**:

$$\mathsf{H} = \sum_{i=1}^{n-1} |p_{i+1} - p_i| \quad \textbf{(4)}$$

with n scaled eigenvector $\underline{\mathbf{e}}_2$ tip path points, with $p_i = q_i + \varepsilon_i \underline{\mathbf{e}}_{2,i}$ where ε_i = ellipticity at the i^{th} bond-path point q_i on the bond-path q.

We name this property the *helicity* length H due the fact that the tips of the scaled $\underline{\mathbf{e}}_2$ eigenvectors will rotate

along the extent of the bond-path between the two bonded nuclei that the bond-path connects.

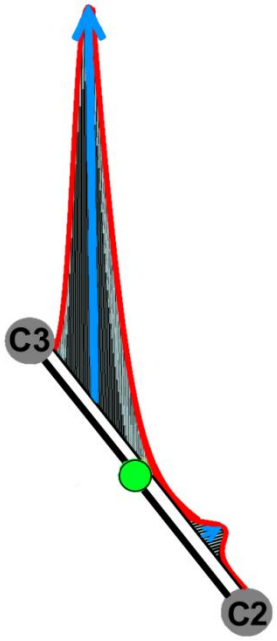

Scheme 1. The red line represents the helical path swept out by the tips of the scaled $\underline{\mathbf{e}}_2$ eigenvectors that we refer to as the helicity length H defined by equation **(4)**. The two blue arrows represented $\underline{\mathbf{e}}_2$ eigenvectors scaled by the ellipticity ε where the vertical scales are exaggerated for visualization purposes. The green sphere indicates the position of the torsional C2-C3 *BCP*.

In the near future we plan a more detailed analysis of the helicity length H^* that includes the $\underline{\mathbf{e}}_1$ eigenvectors in the definition. For now we chose the $\underline{\mathbf{e}}_1$ eigenvector because the associated λ_3 eigenvalue has the largest magnitude. Analogous to the bond-path curvature, see equation **(3)**, we may define dimensionless, *fractional* versions of the helicity length H; several forms are possible and not limited to the following:

$$H_f = (H - BPL)/BPL \qquad (5)$$

We outline in the **Supplementary Materials S5** implementation details of the strategy for obtaining numerically consistent Helicity path lengths H.

The form of H_f defined by equation **(5)** is the closest to the spirit of the bond-path curvature given in equation **(3)**.

Relaxed rotational energy profiles were created using Gaussian 09[34] by varying the ψ_{tyr} Ramachandran angle (herein referred to as θ) between 80 and 110° in steps of 0.5° at the B3LYP[35,36], B3LYP-D3[37], M06-2X[38]and MP2 levels of theory, all with the 6-31+G(d) basis set. The calculations employed Gaussian's "ultrafine" integration grid in the DFT and DFT-D3 calculations.

Calculations of the molecular graphs and critical point properties were performed using AIMAll[39]; all molecular graphs were additionally confirmed to be free of non-nuclear attractor critical points.

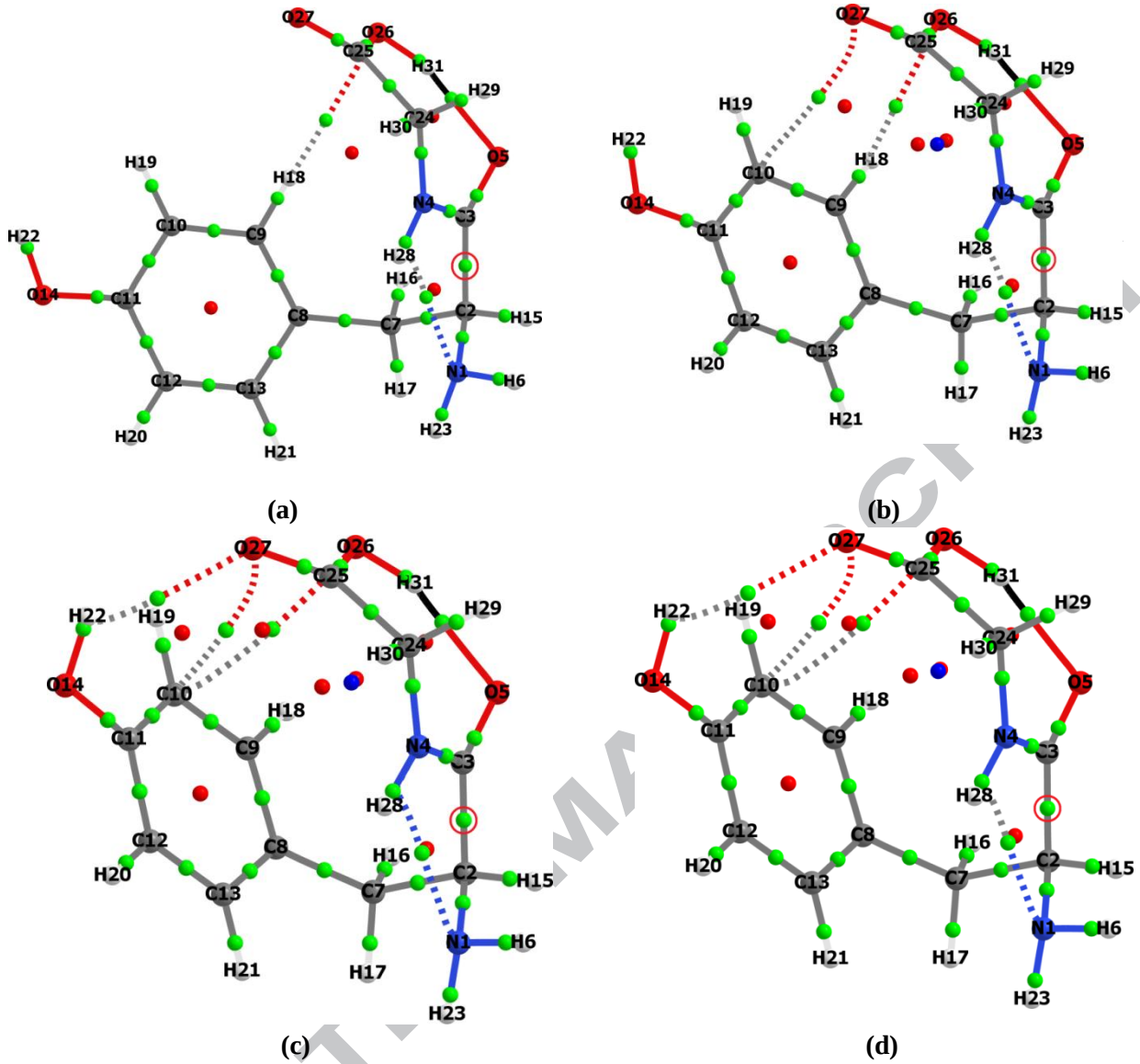

Figure 1. Molecular graphs for the four theory levels B3LYP, B3LYP-D3, M06-2X and MP2 using the 6-31+G(d) basis set for the energy minima are shown in sub-figures **(a-d)** respectively. Plots of the relative energies ΔE are provided in **Supplementary Materials S1**. The atom labels correspond to the molecular graph atom numbering scheme and the torsion C2-C3 *BCP* is indicated by a red circle.

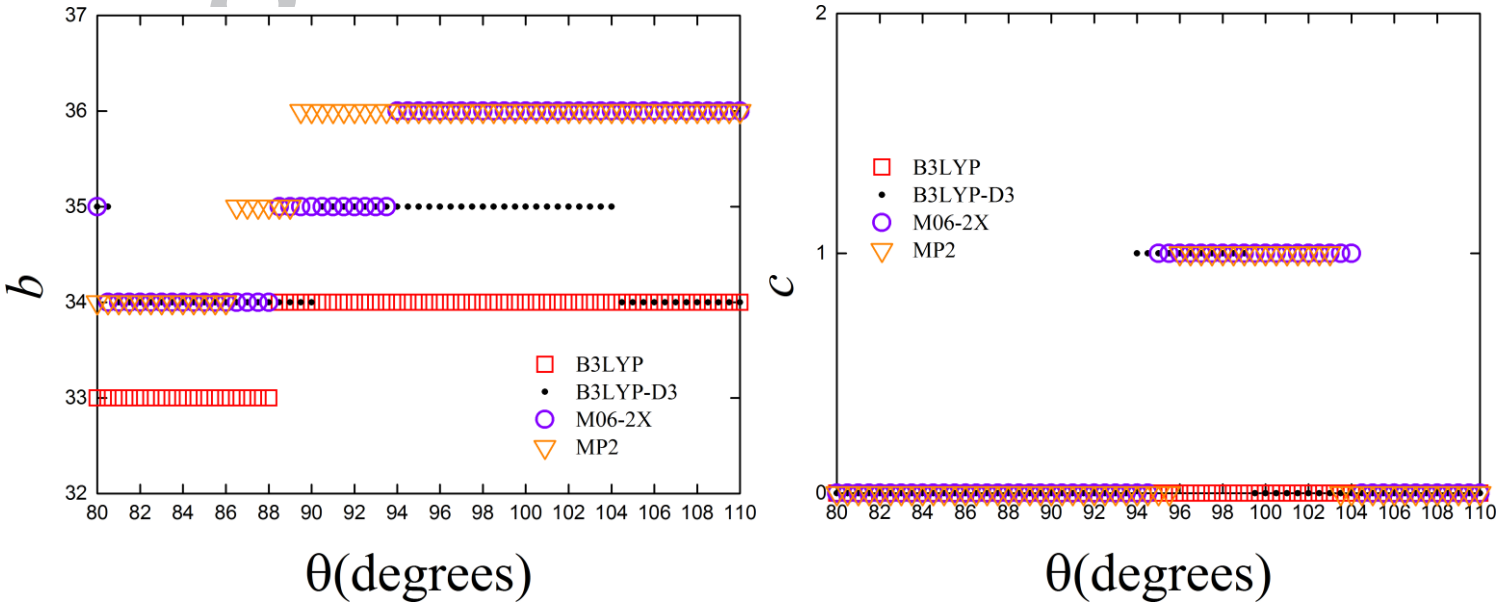

(a) **(b)**

Figure 2. The variation of the numbers of *BCP*s (*b*) and *CCP*s (*c*) with the torsion angle θ for the four levels of theory; MP2, M06-2X, B3LYP and B3LYP-D3 is presented in sub-figures **(a)** and **(b)** respectively.

A known effect of BSSE is that it produces structures that are over bound, i.e. with too much bonding caused by artificial attraction between different parts of the molecule. The B3LYP functional, on the other hand, may have too little bonding due to the inability to describe attractive London dispersion. The degree of bonding can be seen by observing the variation of the number of *BCP*s (*b*) with torsion θ of the molecular graphs of the Tyr-Gly dipeptide obtained with the four levels of theory, see **Figure 2(a)**. The molecular graphs produced from the MP2 and B3LYP calculations comprise the highest and lowest values of *b* respectively. The B3LYP molecular graph contains a maximum of 34 *BCP*s compared with 36 *BCP*s for the MP2 molecular graph. The B3LYP functional, with the lowest minimum value of *b* (*b* = 33) however, may have missed *BCP*s due to the missing attractive London dispersion. The number of *BCP*s of the B3LYP-D3 molecular graphs falls in between those of MP2 and B3LYP, with a minimum and maximum of 34 *BCP*s and 35 *BCP*s respectively. This is consistent with previous non-QTAIM investigations where MP2 generally produced more folded Tyr-Gly dipeptide conformers than B3LYP, indicating a larger degree of bonding between different parts of the molecule[1,3].

In this investigation we can see that the B3LYP-D3, M06-2X and MP2 levels of theory generate molecular graphs with compact 3-D_{QT} quantum topologies in the vicinity of the energy minimum at θ = 96° as evidenced by the presence of a *CCP*, see **Figure 2(b)**. Conversely, use of B3LYP produces an open 2-D_{QT} molecular graph. More compact structures are associated with more bonding between different parts of the molecule, and thus, the more open structure predicted by B3LYP may be a result of lacking dispersion or due to larger BSSE in the MP2 (and M06-2X) calculations. As the D3 add-on in B3LYP-D3 does not add BSSE, the more compact B3LYP-D3 structure must be due to dispersion. The even more compact MP2 structure, however, could in addition be due to BSSE. The plots of the variation of the relative energies ΔE with the torsion θ are provided in the **Supplementary Materials S1**.

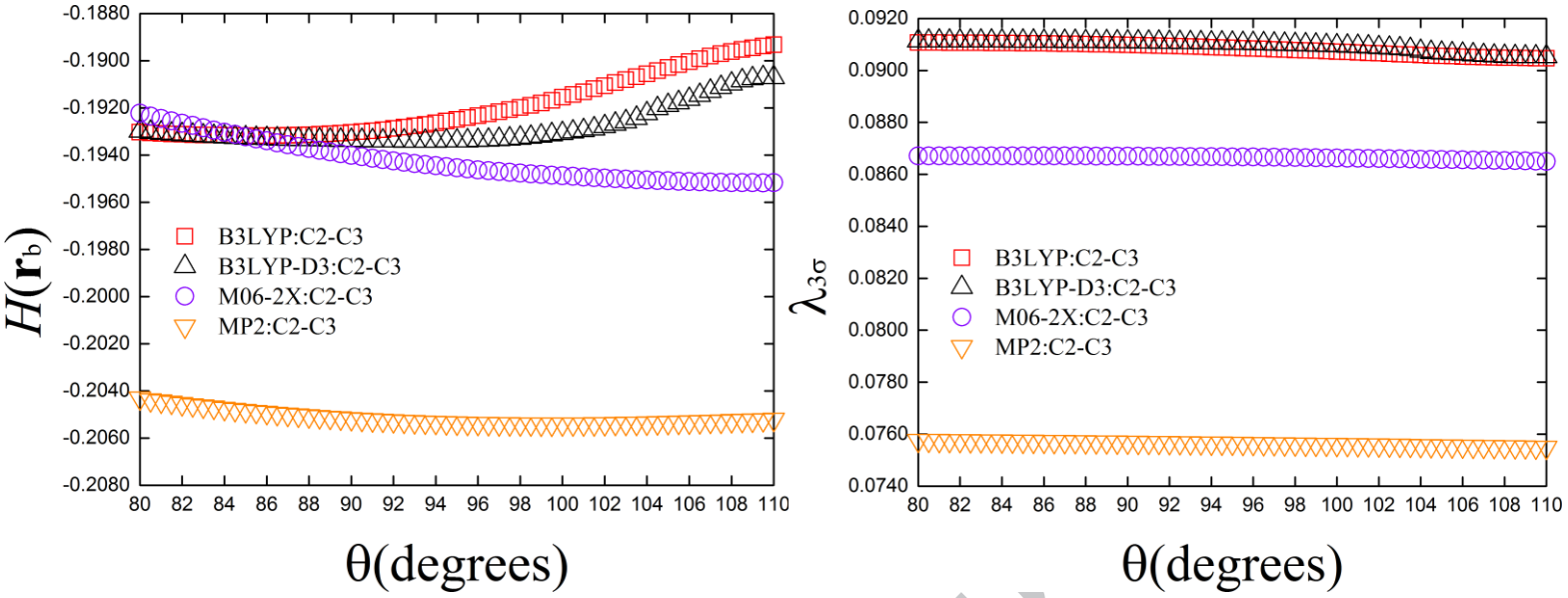

(a) **(b)**

Figure 3. The variation of the total local energy density $H(\mathbf{r_b})$ (in a.u.) and the stress tensor eigenvalue $\lambda_{3\sigma}$ of the torsional C2-C3 *BCP* with the torsion θ for the four theory levels are presented in sub-figures **(a)** and **(b)** respectively; see **Figure 1** for details of the atomic labeling scheme. Additional plots of the ellipticity ε, the total local energy density $H(\mathbf{r_b})$ and $\lambda_{3\sigma}$ that also include the closed-shell *BCP*s are provided in **Supplementary Materials S2-S4** respectively.

The order of increasing *BCP* strength of the torsional C2-C3 *BCP* as indicated by the total local energy density $H(\mathbf{r_b})$ from the four levels of theory in the vicinity of the energy minima at 96° is MP2 < M06-2X < B3LYP-D3 < B3LYP, see **Figure 3(a)**. This is consistent with the order of decreasing magnitude of the BSSE[5]. There is a similar trend for the stress tensor eigenvalue $\lambda_{3\sigma}$, which indicates that the torsional C2-C3 *BCP* stability is lowest for the MP2 calculations and highest for B3LYP-D3 and B3LYP, which are very close in value to each other, see **Figure 3(b)**.

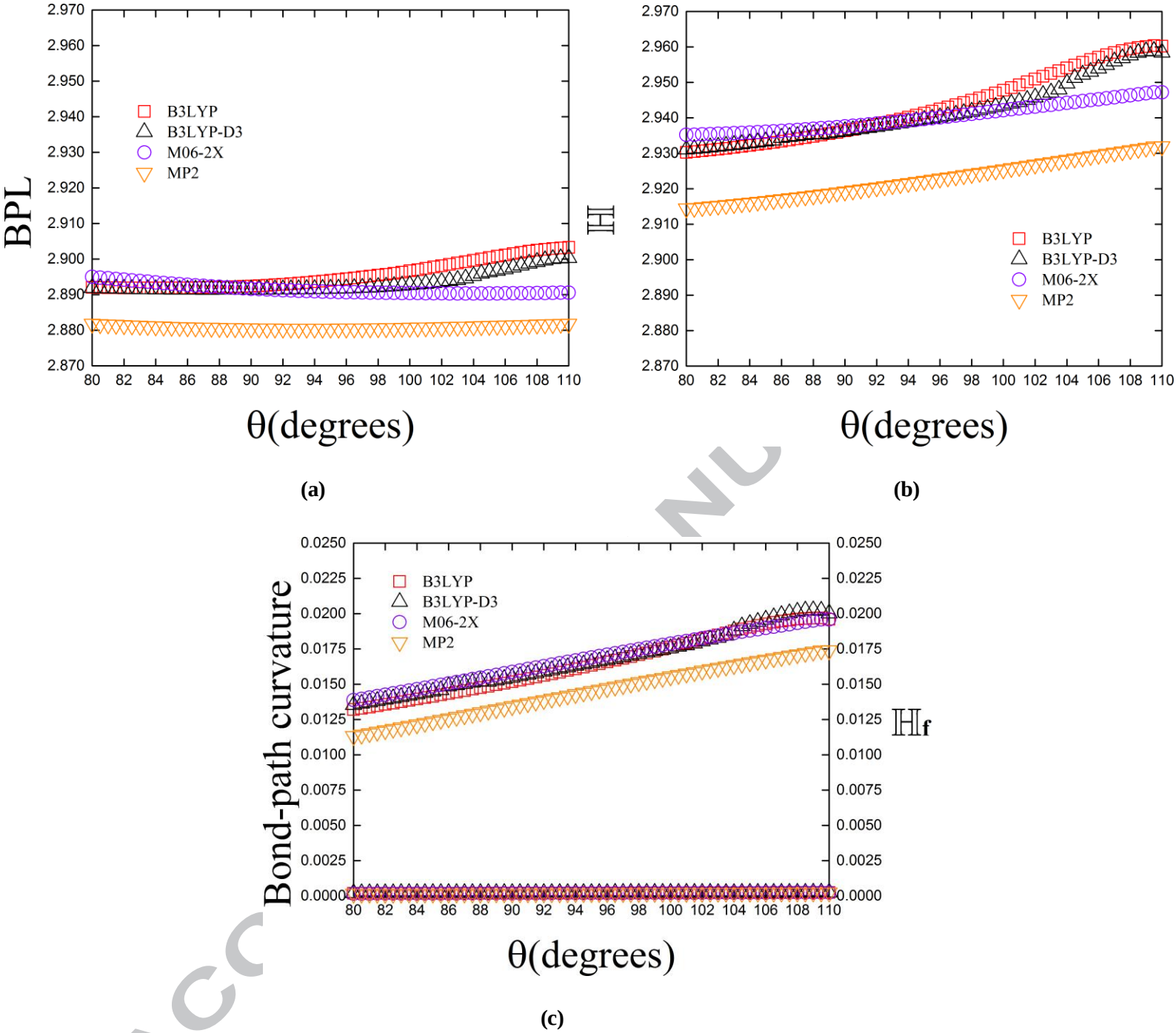

Figure 4. The variation of the bond-path lengths (BPL) in a.u. of the torsional C2-C3 *BCP* with torsion angle θ for the four levels of theory is shown in sub-figure **(a)**. The helicity length H of the torsional C2-C3 *BCP* is shown in sub-figure **(b)**, see also the **Supplementary Materials S5**. The corresponding variation of the bond-path curvature and H_f = (H – BPL)/BPL are presented together in sub-figures **(c)**.

The minimum values of the bond-path length defined as BPL_{min} in a.u. and the corresponding value of torsion helicity length H; are B3LYP (2.892,84.0º), B3LYP-D3 (2.891,87.0º), M06-2X (2.890,104.5º) and MP2 (2.880,93.0º). The value of the BPL is lowest for the torsional C2-C3 *BCP* of the molecular graph obtained from MP2 calculations and highest with the B3LYP calculations, see **Figure 4(a)**. This result is consistent with the results for the total local energy density $H(\mathbf{r_b})$, see **Figure 2(a)**. The bond-path curvature is also provided; in this case it is four orders of magnitude lower than the BPL and therefore negligible. It

can be seen that the helicity length H of the torsional C2-C3 *BCP* displays a greater range of values than the BPL, see **Figure 4(a)** and **Figure 4(b)** respectively. The helicity length H for the MP2 calculations maintains a constant level of 2.94 a.u. for the entire range of the torsion θ in contrast to the other three levels of theory, see **Figure 4(b)**. The dimensionless fractional helicity measure H_f produced characteristically different results for each of the four levels of theory, see **Figure 4(c)**. Similar results are seen for these four levels of theory with the def2-TZVP basis set, see the **Supplementary Materials S6**.

We have used QTAIM and the stress tensor to provide a detailed analysis of the topology of the molecular graph, *BCP* and bond-path properties including the newly introduced helicity length H of a Tyr-Gly dipeptide conformer subjected to a torsion θ with four levels of theory; MP2, M06-2X, B3LYP-D3 and B3LYP and a modest sized basis set, 6-31+G(d). The plots of the number of *BCP*s, *b*, versus the torsion θ indicated that the MP2 and B3LYP levels of theory comprised the highest and lowest numbers of *BCP*s, respectively. The degree of structural compactness was determined with plots of the numbers of *CCP*s, *c*, versus the torsion θ. The Tyr-Gly conformer obtained using B3LYP was found to possess, for all values of torsion θ, 2-D_{QT} molecular graphs, demonstrating the previously suspected 'floppy' structure. In addition we also found from the stress tensor $\lambda_{3\sigma}$ that the stability of the torsional C2-C3 *BCP* was lowest when using MP2 calculations. The newly introduced helicity length H demonstrated that the MP2 calculations produced a unique and presumably unwanted behavior on the basis of the previously determined large BSSE value, in the form of a negligible response to the torsion θ that was not seen for the M06-2X, B3LYP-D3 and B3LYP theory levels. We suggest that these QTAIM and stress tensor tools can be used in the future, subject to further investigations, without needing to default to using very large basis sets with a high level of theory or needing to calculate the BSSE.

Acknowledgements

The National Natural Science Foundation of China is gratefully acknowledged, project approval number: 21673071. The One Hundred Talents Foundation of Hunan Province and the aid program for the Science and Technology Innovative Research Team in Higher Educational Institutions of Hunan Province are also gratefully acknowledged for the support of S.J. and S.R.K. TvM and HF thank EaStCHEM for support through the EaStCHEM Research Computing Facility.

References

1. Holroyd, L. F. & van Mourik, T. Insufficient description of dispersion in B3LYP and large basis set superposition errors in MP2 calculations can hide peptide conformers. *Chem. Phys. Lett.* **442,** 42–46 (2007).

2. Shields, A. E. & van Mourik, T. Comparison of ab Initio and DFT Electronic Structure Methods for

Peptides Containing an Aromatic Ring: Effect of Dispersion and BSSE. *J. Phys. Chem. A* **111,** 13272–13277 (2007).

3. van Mourik, T., Karamertzanis, P. G. & Price, S. L. Molecular Conformations and Relative Stabilities Can Be as Demanding of the Electronic Structure Method as Intermolecular Calculations. *J. Phys. Chem. A* **110,** 8–12 (2006).
4. Toroz, D. & Mourik, T. van. The structure of the gas-phase tyrosine–glycine dipeptide. *Mol. Phys.* **104,** 559–570 (2006).
5. Rabia Hameed, Afsar Khan and Tanja van Mourik. *Mol. Phys. in press* (2017).
6. Jensen, F. Using valence bond methods to estimate intramolecular basis set superposition errors. *J. Chem. Phys.* **146,** 184109 (2017).
7. Palermo, N. Y., Csontos, J., Owen, M. C., Murphy, R. F. & Lovas, S. Aromatic-backbone interactions in model α-helical peptides. *J. Comput. Chem.* **28,** 1208–1214 (2007).
8. Mourik, T. V. Comment on "Aromatic-Backbone Interactions in Model α-Helical Peptides" [Palermo et al., J Comput Chem 2007, 28, 1208]. *J. Comput. Chem.* **29,** 1–3 (2008).
9. Csontos, J., Palermo, N. Y., Murphy, R. F. & Lovas, S. Reply to "Comment on Aromatic-Backbone Interactions in Model α-Helical Peptides". *J. Comput. Chem.* **29,** 4–7 (2008).
10. Kruse, H. & Grimme, S. A geometrical correction for the inter- and intra-molecular basis set superposition error in Hartree-Fock and density functional theory calculations for large systems. *J. Chem. Phys.* **136,** 154101 (2012).
11. Asturiol, D., Duran, M. & Salvador, P. Intramolecular basis set superposition error effects on the planarity of benzene and other aromatic molecules: A solution to the problem. *J. Chem. Phys.* **128,** 144108 (2008).
12. Jensen, F. An Atomic Counterpoise Method for Estimating Inter- and Intramolecular Basis Set Superposition Errors. *J. Chem. Theory Comput.* **6,** 100–106 (2010).

13. Bader, R. F. W. *Atoms in Molecules: A Quantum Theory*. (Oxford University Press, USA, 1994).

14. Jenkins, S. & Morrison, I. Characterization of Various Phases of Ice on the Basis of the Charge Density. *J. Phys. Chem. B* **103,** 11041–11049 (1999).

15. Bader, R. F. W. A Bond Path: A Universal Indicator of Bonded Interactions. *J. Phys. Chem. A* **102,** 7314–7323 (1998).

16. Bader, R. F. W. Bond Paths Are Not Chemical Bonds. *J. Phys. Chem. A* **113,** 10391–10396 (2009).

17. Collard, K. & Hall, G. G. Orthogonal trajectories of the electron density. *Int. J. Quantum Chem.* **12,** 623–637 (1977).

18. Johnson, C. K. Peaks, Passes, Pales, and Pits: A Tour Through the Critical Points of Interest in a Density Map. in *Abstracts of the American Crystallographic Association* 30 (ACA Publications, Inc., 1977).

19. Smith, V. H., Price, P. F. & Absar, I. XVI. Representations of the Electron Density and its Topographical Features. *Isr. J. Chem.* **16,** 187–197 (1977).

20. Jenkins, S. Quantum topology phase diagrams for molecules, clusters, and solids. *Int. J. Quantum Chem.* **113,** 1603–1608 (2013).

21. Jenkins, S., Restrepo, A., David, J., Yin, D. & Kirk, S. R. Spanning QTAIM topology phase diagrams of water isomers W4, W5 and W6. *Phys. Chem. Chem. Phys.* **13,** 11644–11656 (2011).

22. Jenkins, S., Rong, C., Kirk, S. R., Yin, D. & Liu, S. Spanning Set of Silica Cluster Isomer Topologies from QTAIM. *J. Phys. Chem. A* **115,** 12503–12511 (2011).

23. Xu, T., Jenkins, S., Xiao, C.-X., Maza, J. R. & Kirk, S. R. The Pt site reactivity of the molecular graphs of Au6Pt isomers. *Chem. Phys. Lett.* **590,** 41–45 (2013).

24. Kraka, E. & Cremer, D. Description of chemical reactions in terms of the properties of the electron density. *J. Mol. Struct. THEOCHEM* **255,** 189–206 (1992).

25. Jenkins, S., Blancafort, L., Kirk, S. R. & Bearpark, M. J. The response of the electronic structure to electronic excitation and double bond torsion in fulvene: a combined QTAIM, stress tensor and MO

perspective. *Phys. Chem. Chem. Phys.* **16,** 7115–7126 (2014).

26. Guevara-García, A. *et al.* Pointing the way to the products? Comparison of the stress tensor and the second-derivative tensor of the electron density. *J. Chem. Phys.* **134,** 234106 (2011).
27. Ayers, P. W. & Jenkins, S. An electron-preceding perspective on the deformation of materials. *J. Chem. Phys.* **130,** 154104 (2009).
28. S. Jenkins, A. G. García, P. W. Ayers, S. R. Kirk, E. Echegaray, A. Labbe. in *In Electronic Effects in Organic Chemistry* (ed. Kirchner, B.) 1–22 (Springer Berlin Heidelberg, 2011).
29. Bader, R. F. W. Quantum topology of molecular charge distributions. III. The mechanics of an atom in a molecule. *J. Chem. Phys.* **73,** 2871–2883 (1980).
30. Bader, R. F. W. & Nguyen-Dang, T. T. Quantum Theory of Atoms in Molecules–Dalton Revisited. in *Advances in Quantum Chemistry* (ed. Löwdin, P.-O.) **14,** 63–124 (Academic Press, 1981).
31. Wang, L. *et al.* QTAIM and Stress Tensor Characterization of Intramolecular Interactions Along Dynamics Trajectories of a Light-Driven Rotary Molecular Motor. *J. Phys. Chem. A* **121,** 4778–4792 (2017).
32. Jenkins, S. & Heggie, M. I. Quantitative analysis of bonding in 90° partial dislocation in diamond. *J. Phys. Condens. Matter* **12,** 10325 (2000).
33. Jenkins, S. & Morrison, I. The chemical character of the intermolecular bonds of seven phases of ice as revealed by ab initio calculation of electron densities. *Chem. Phys. Lett.* **317,** 97–102 (2000).
34. Frisch, M. *et al. Gaussian 09, Revision B.01*. (Gaussian, Inc., 2009).
35. Becke, A. D. Density-functional exchange-energy approximation with correct asymptotic behavior. *Phys. Rev. A* **38,** 3098–3100 (1988).
36. Becke, A. D. Density ‐ functional thermochemistry. III. The role of exact exchange. *J. Chem. Phys.* **98,** 5648–5652 (1993).
37. Grimme, S., Antony, J., Ehrlich, S. & Krieg, H. A consistent and accurate ab initio parametrization of

density functional dispersion correction (DFT-D) for the 94 elements H-Pu. *J. Chem. Phys.* **132,** 154104 (2010).

38. Zhao, Y. & Truhlar, D. G. The M06 suite of density functionals for main group thermochemistry, thermochemical kinetics, noncovalent interactions, excited states, and transition elements: two new functionals and systematic testing of four M06-class functionals and 12 other functionals. *Theor. Chem. Acc.* **120,** 215–241 (2008).
39. Keith, T. A. *AIMAll, Revision 17.01.25*. (TK Gristmill Software, 2017).

Highlights

- Tyr-Gly dipeptide subjected to a torsion for MP2, M06-2X, B3LYP and B3LYP-D3.
- Quantum topology phase diagrams quantified changes in bonding topology with torsion.
- Introduced QTAIM helicity length H for Tyr-Gly dipeptide conformer.
- QTAIM and stress tensor reflect differences in MP2, M06-2X, B3LYP and B3LYP-D3.
- Helicity length H demonstrated that MP2 produced a unique response to the torsion.

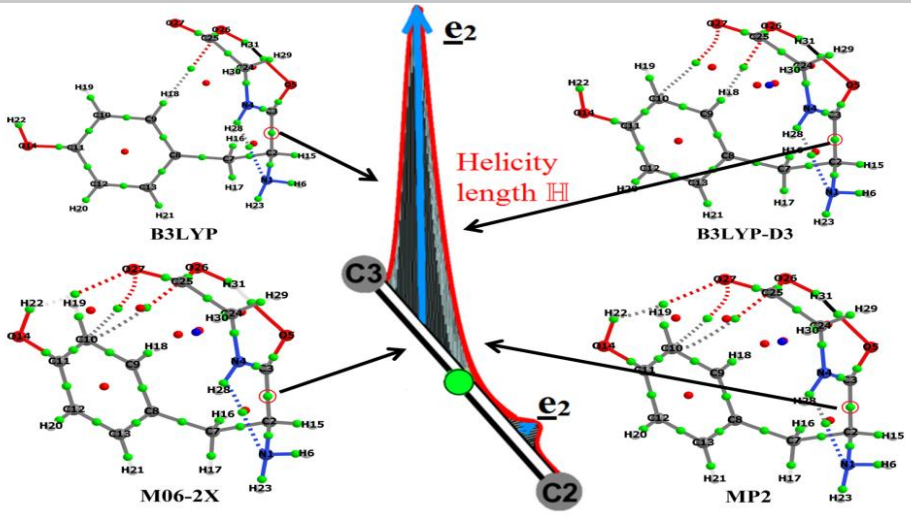

Graphical abstract